11HSD1 deficiency or inhibition enhances hepatic myofibroblast activation in murine liver fibrosis

11βHSD1 deficiency or inhibition enhances hepatic myofibroblast activation in murine liver fibrosis.

Zou X[1,2,4], Ramachandran P[2,4], Kendall TJ[2], Pellicoro A[2], Dora E[2], Aucott RL[2], Manwani K[1], Man TY[1], Chapman KE[1], Henderson NC[2], Forbes SJ[3], Webster SP[1], Iredale JP[2], Walker BR[1], Michailidou Z[1,2*]

Author Affiliations: [1] The University of Edinburgh /BHF Centre for Cardiovascular Science; [2] The University of Edinburgh/ MRC Centre for Inflammation Research, [3] The University of Edinburgh/MRC Centre for Regenerative Medicine, Queen's Medical Research Institute, 47 Little France Crescent, Edinburgh EH16 4TJ, UK.[4] these authors contributed equally.

***Corresponding Author: Zoi Michailidou,** v1zmicha@staffmail.ed.ac.uk

Key words: glucocorticoids, macrophages, collagen, carbon tetrachloride

List of Abbreviations.

ALT alanine aminotransferase

AST aspartate aminotransferase

GC glucocorticoids

11βHSD1 11beta-hydroxysteroid dehydrogenase-1

HSC hepatic stellate cells

MFB hepatic myofibroblasts

NASH: Non-alcoholic steatohepatitis

Financial Support. This work was funded by the British Heart Foundation (BRW), a Henry Wellcome Postdoctoral Fellowship (ZM; 085458/Z/08/Z) and a British Heart Foundation/University of Edinburgh Centre of Research Excellence Transition Award Fellowship (ZM). Mice were generated under a Wellcome Trust Programme Grant 08318/4/Z/07/Z (to JR Seckl, JS Savill, KE Chapman, JJ Mullins and BRW). UE2316 was

generated with a Wellcome Trust Seeding Drug Discovery award (SPW and BRW). Xiantong Zou was supported by the Chinese Scholarship Council.

2-sentence Summary of Manuscript:

11βHSD1 inhibition regulates hepatic myofibroblast activation and enhances the fibrotic response following liver injury.

Abstract

A hallmark of chronic liver injury is fibrosis, with accumulation of extracellular matrix orchestrated by activated hepatic stellate cells (HSCs). Glucocorticoids (GC) limit HSC activation in vitro and tissue GC levels are amplified by 11beta-hydroxysteroid dehydrogenase-1 (11βHSD1). Although 11βHSD1 inhibitors have been developed for type 2 diabetes mellitus and improve diet-induced fatty liver in various mouse models, effects on the progression and/or resolution of liver injury and consequent fibrosis have not been characterised. Here we have used the reversible carbon tetrachloride-induced model of hepatocyte injury and liver fibrosis to show that in 2 models of genetic 11βHSD1 deficiency (global; *Hsd11b1*$^{-/-}$ and hepatic myofibloblast-specific; *Hsd11b1*$^{fl/fl}$ /Pdgfrb-cre) and 11βHSD1 pharmacological inhibition in vivo exacerbates hepatic myofibroblast (MFB) activation and liver fibrosis. In contrast, liver injury and fibrosis in hepatocyte-specific *Hsd11b1*$^{fl/fl}$/albumin-cre mice did not differ from that of controls, ruling out 11βHSD1 deficiency in hepatocytes as the cause of the increased fibrosis. In primary hepatic stellate cell (HSC) culture, glucocorticoids inhibited expression of the key profibrotic genes *Acta2* and *Col1α1*, an effect attenuated by the 11βHSD1 inhibitor UE2316. HSCs from *Hsd11b1*$^{-/-}$ and *Hsd11b1*$^{fl/fl}$ /Pdgfrb-cre mice expressed higher levels of *Acta2* and *Col1α1* and were correspondingly more potently activated. *In vivo* UE2316 administration prior to chemical injury recapitulated findings in *Hsd11b1*$^{-/-}$ mice, including greater fibrosis. ***Conclusion:*** 11βHSD1 deficiency enhances MFB activation and promotes initial fibrosis following chemical liver injury. Hence, the effects of 11βHSD1 inhibitors on liver injury and repair are likely to be context-dependent and deserve careful scrutiny as these compounds are developed for chronic diseases including metabolic syndrome and dementia.

The prevalence of chronic liver disease is increasing globally. Regardless of the underlying cause, alcohol, metabolic disease or non-alcoholic steatohepatitis (NASH), hepatic damage results in fibrosis- a dynamic process characterized by accumulation of extracellular matrix (1). Activated hepatic stellate cell/ myofibroblasts (HSC/MFB) are the major source of extracellular matrix in mouse liver fibrosis models (1-2), while scar associated macrophages facilitate the spontaneous resolution of liver fibrosis (3). The severity of fibrosis, for example in NASH patients, is correlated with adverse clinical outcomes (4-5). Currently there is no effective regime to limit fibrosis without adversely affecting repair (4), therefore, novel disease-modifying anti-fibrotic therapies are needed.

Glucocorticoids have wide ranging actions that modulate many of the pathological processes that occur during tissue injury and repair and which contribute to liver fibrosis (6). Tissue glucocorticoid levels are regulated by the intracellular enzyme 11βHSD1 that converts inactive cortisone into active cortisol in humans (or 11dehydro-corticosterone into corticosterone in mice) and is highly abundant in liver (7). 11βHSD1 influences hepatic lipid accumulation, with transgenic 11βHSD1 overexpression in liver leading to hepatic steatosis and dyslipidemia while 11βHSD1 deficiency protects from hepatic steatosis on a high fat diet (8-9). However, little is known of the role of 11βHSD1 in liver fibrosis. One observational study showed no association between liver 11βHSD1 expression and the pathology of fatty liver or NASH in humans (10). In contrast, another study showed that in early stages of NAFLD, with steatosis alone, hepatic 11βHSD1 activity is reduced whereas progression to NASH was associated with increased 11βHSD1 levels (11).

Importantly, 11βHSD1 inhibitors have been developed and shown to be moderately efficacious in Phase 2 clinical trials in patients with type 2 diabetes (12). Moreover, a recent study showed that administration of the 11βHSD1 inhibitor RO5093151 in NAFLD patients reduced liver lipid content (13). Given the potential use of 11βHSD1 inhibitors as a therapy in patients either at risk of NAFLD or with established hepatic steatosis, it is imperative to understand the influence of 11βHSD1 on liver fibrosis.

In this study, we sought to define the direct effects of limiting liver glucocorticoid availability on hepatic fibrosis, independent of metabolic functions. We therefore, utilized global, hepatocyte-specific and stellate/myofibroblast-specific 11βHSD1 deficient mice and a

specific small molecule 11βHSD1 inhibitor, to study the functional role of 11βHSD1 in murine models of toxin-induced liver fibrosis. We demonstrate, for the first time, that 11βHSD1 deficiency or inhibition promotes MFB activation and liver fibrogenesis in the CCl_4 model.

Materials and Methods

Mouse liver fibrosis models. All experiments involving animals were approved by The University of Edinburgh Animal Welfare and Ethical Review Body and by the United Kingdom Home Office. Experiments used adult male (14 weeks of age) mice with global deficiency (*Hsd11b1*$^{-/-}$; GKO) (14). The GKO mice have been backcrossed for over 10 generations on a C57Bl/6J genetic background and C57Bl/6J mice were used as controls (15-18). GKO were maintained in parallel with the control C57Bl/6J; both lines were bred and maintained within our biomedical research facility housed under standard conditions. To avoid inter-animal variability that would be introduced due to differences in the stage of estrous in females, only male mice were used. Male mice (12 weeks of age) in which deletion was targeted to hepatocytes (LKO) were generated by crossing *Albumin-Cre*$^{Tg/+}$ mice (B6.Cg-Tg(Alb-cre)21Mgn/J; Jackson Laboratories) with mice homozygous for a "floxed" allele of *Hsd11b1* (*Hsd11b1*$^{fl//fl}$) in which exon 3 is flanked by *LoxP* sites (generated by Artemis Pharmaceuticals directly onto a C57BL/6 background and designated *Hsd11b1*^{tm1Arte}, MGI 5784734). Cre-mediated excision of exon 3 generates a null allele (19). *Cre*$^{-}$ *Hsd11b1*$^{fl//fl}$ littermates served as controls for LKO mice. To target deletion specifically at myofibroblast/stellate cells (MFKD) , *Hsd11b1*$^{fl//fl}$ mice were crossed with *the platelet-derived growth factor receptor beta (Pdgfrb)-Cre*$^{Tg/+}$ mice (20). *Cre*$^{-}$ *Hsd11b1*$^{fl//fl}$ littermates served as controls for MFKD mice.

Carbon tetrachloride (CCl_4) model. Mouse chronic liver fibrosis was induced by i.p. injection of 25% CCl_4/g twice weekly for 12 weeks. Male GKO or LKO and their control littermates were culled at 24 hours (peak fibrosis), 72 hours, 1 week and 1 month (scar resolution phases) after the last injection, as previously validated (3). MFKD male mice were culled 24h after the last CCl4 injection to evaluate the role of 11βHSD1 deficiency at the peak fibrotic response. For acute injury, a single dose of 25% CCl4 / g ip was given in GKO or control mice and livers and plasma were collected after 24h.

In male C57Bl/6J mice, pharmacological 11βHSD1 inhibition was achieved by mixing chow diet with 0.15% UE2316 ([4-(2-chlorophenyl-4-fluoro-1-piperidinyl][5-(1H-pyrazol-4-yl)-3-thienyl]-methanone). Groups of C57Bl6/J mice were given either a chow diet (CD) or diet containing UE2316 (UE) ad libitum (21) either throughout 12 weeks of CCl_4 administration and until sacrifice, or only from 48h after the last CCl_4 injection until sacrifice, ie during resolution (UE-R). Mice were sacrificed at 6 hours, 24 hours, 72 hours and 8 days after the last CCl_4 injection.

Alternative liver pathology models. An alternative model of liver fibrosis was induced in C57Bl/6J mice by administration of thioacetamide (TAA; 600 mg/L) in drinking water for 1 year. Livers were harvested 24 hours or 1 week after TAA termination. To induce steatosis and NASH in a model of NAFLD, GKO male mice and age-matched C57Bl/6J mice aged 6-10 months were fed commercially available diets (all from Dyets, Bethlehem, PA, US): control (Con, 518574), choline deficient (CDD, 518753) or methionine-choline deficient (MCDD, 518810), for 2 weeks as previously described (22).

Isolation of non-parenchymal liver cells and flow cytometry. Fresh liver was perfused with 5 ml saline via the portal vein and 100-300 mg then digested with RPMI1640 medium with Dnase I and Collagenase IV at 37^{o}C. After digestion, hepatocytes were pelleted and discarded by centrifugation at 50g for 5 minutes. Non-parenchymal cells were washed with RPMI 1640 medium and pelleted by centrifugation at 350g for 15 minutes, then washed and blocked with 10% mouse serum for 30 minutes. Antibodies against CD11b (clone M1/70; Ebioscience, Hatfield, UK), Ly-6C (clone HK1.4; Ebioscience), CD45.2 (clone 104; Ebioscience), F4/80 (dilution 1:50; clone BM8; Invitrogen), Ly-6G (clone 1A8; Biolegend, San Diego, CA,US) were added for 30 minutes, in a dilution of 1:100 unless specified. Cell viability was assessed with Fixable Viability Dye eFluor780 (Ebioscience) according to the manufacturer's protocols. Cells were formalin fixed and analysed by flow cytometry using a BD LSR Fortessa II (BD Bioscience, Oxford, UK).

Immunofluorescence and immunochemistry. For immunohistochemistry, livers were fixed with formalin for 16 hours directly after harvest. 4μm sections were de-waxed and rehydrated

followed by antigen retrieval in boiling sodium citrate. Avidin and Biotin were blocked according to the manufacturer's protocol (Vector, Peterborough, UK). Protein block (DAKO, Cambridge, UK) or serum was added and sections were then incubated with αSMA (Sigma Aldrich, Dorset, UK) or collagen I or GR1(Ly6G) (Cambridge bioscience, Cambridge, UK) or F4/80 (Abcam, Cambridge, UK) or Reelin (Abcam, Cambridge, UK) antibodies at 4^{o}C overnight and subsequent secondary antibody for 30 minutes. After ABC vector incubation, the sections were incubated with DAB for 10 minutes, counter stained with haematoxylin. Picrosirius red staining (PSR) was performed as previously described (3,23) . 30–40 high power fields (magnification ×80) per section were randomly selected for each slide by an assessor blind to genotype. Images were analysed in Photoshop CS3 for positive stained pixels and normalized to total number of pixels. In the Period Acid-Schiff (PAS) stain, necrotic cell area was quantified in a blinded manner using Image J Trainable Weka Segmentation tool.

Liver Histopathology. Blinded hematoxylin and eosin (H&E) stained sections from the acute single dose CCl4 and the chronic CCl4 injury models (at 24h peak fibrosis) were evaluated by a pathologist using 2 separate ordinal scales.; Inflammation was scored using the inflammation component of the NAS scoring system for NASH (24) (0 – no inflammation; 1 - <2 necroinflammaoty foci/20x field; 2 – 2-4 necroinflammatory foci/20x field; 3 - >4 necroinflammatory foci/20x field). Hepatocellular necrosis was scored using a scale based on the descriptors of severity used in the reporting of acute lobular hepatitis in human biopsies (0 – none; 1 – single cell necrosis; 2 – confluent necrosis; 3 – zonal necrosis; 4 – panacinar necrosis). The data are ordered categorical and therefore are presented as dotplots.

Primary culture of mouse hepatic stellate cells. Livers from GKO, C57BL/6J controls, MFKO and control littermate mice were perfused with 5ml HBSS+, excised, cut into 2x2 mm^2 cubes and digested in HBSS medium supplemented with DNAse I, Collagenase IV and Pronase. Released cells were purified through a 70μm strainer and separated by density gradient centrifugation in sequential concentrations of OptiPrep (Sigma Aldrich, Dorset, UK). 1x10^6 cells/well were plated and cultured in DMEM with 16% FBS, 1% penicillin/streptomycin. HSCs were left to spontaneously activate then were collected after 2, 5, 8, or 11d in culture for mRNA and protein analysis. Pharmacological 11βHSD1 inhibition

was performed in primary cultures of C57Bl/6J HSCs. HSCs were treated with vehicle (DMSO), 500nM corticosterone, 500nM 11-dehydrocorticosterone and/or 10μM UE2316. HSC medium was replaced daily and all treatments were added daily with the medium change, for the duration of the experiment. Following 8d of treatment, HSCs were collected for mRNA and protein analysis.

Other Standard Methods: Immunoblotting, RNA extraction, real time PCR, 11βHSD1 activity assay and In situ hybridization have been described before (25,26,27) and detailed methods can be found in Supporting Information.

Statistical Analysis. All data are expressed as mean+/- SEM. Statistical analysis was performed using Graphpad prism or Statistica 7. 2-way ANOVA was used to test for the interaction of genotype/treatment analysis. 2-tailed unpaired Student's *t* test or one-way ANOVA was used for the comparison of 2 (ie control versus KO mice) or 3 groups respectively (ie .control, CD, MCD diet comparisons).

Results

11βHSD1 expression is reduced during hepatic injury

In the carbon tetrachloride (CCl_4) murine model of liver fibrosis, whole liver 11βHSD1 mRNA (Fig. 1A) and protein levels (Fig. 1B) were reduced during injury. This injury-associated reduction in whole liver 11βHSD1 mRNA, was recapitulated in both the thioacetamide (TAA) (Fig. 1C) model of liver fibrosis, and in the CDD and MCDD models of steatosis and NASH (Fig. 1D). 11βHSD1 activity levels were not significantly altered during peak CCl_4-induced fibrosis (Supporting Fig. S1A). During the scar resolution phase following CCl_4 injury, 11βHSD1 mRNA and protein levels returned to levels seen in uninjured (vehicle-treated) mice (Fig. 1A-B).

11βHSD1 is expressed in hepatic stellate cells, attenuating their activation *in vitro*

Although 11βHSD1 is highly expressed in hepatocytes, the key cells orchestrating fibrogenesis in parenchymal liver injury models are the hepatic stellate cells (HSCs). HSCs

are "spontaneously" activated in culture such that αSMA (a global marker of spontaneous HSC activation *in vitro*) protein levels are maximal at day 8 (Fig. 2A). Significant 11βHSD1 expression was detectable in primary murine HSCs, with a striking reduction observed in 11βHSD1 mRNA (Fig. 2B), protein (Fig. 2C) and activity (Fig. 2D) following spontaneous HSC activation (day 8) *in vitro*. Similarly, 11βHSD1 gene expression was present in the human LX-2 (28) HSC cell line, and was significantly reduced in response to activation with TGF-β, a classic pro-fibrogenic stimulus (Supporting Fig. S1B).

To investigate the functional role of 11βHSD1 in HSC activation, primary HSCs were isolated from GKO (11βHSD1-deficient) mice and showed significantly higher *Acta2* (Fig. 2E) and *Col1a1* (Fig. 2F) mRNA levels at day 8 compared to control HSCs.

Consistent with this effect of 11βHSD1 being mediated by amplification of glucocorticoids, incubation of wild-type murine HSCs with either corticosterone or 11dehydro-corticosterone, the inert substrate for 11βHSD1, reduced *Acta2* (Fig.3A) and *Col1a1* (Fig.3B) mRNA levels. The effects of 11dehydro-corticosterone were abrogated by co-administration of the specific 11βHSD1 inhibitor UE2316 (Fig. 3A, 3B).

Global 11βHSD1 deficient mice show increased hepatic myofibroblast activation following CCl4 injury

To investigate whether reducing 11βHSD1 (in GKO mice) *in vivo* enhances MFB/HSC activation and delays the resolution of scarring, we utilized the reversible CCl_4 liver fibrosis model because the times of peak injury and maximal scar resolution have been previously well defined; time points were chosen to reflect the injury and resolution phases since collagen deposition is higher at 24h and resolving after 72h (3). After 12 weeks of CCl_4 treatment, GKO mice showed significantly higher picrosirius red staining (Fig. 4A) and collagen I deposition (Supporting Fig.S2A) at peak (24h) fibrosis. Increased fibrogenesis in the absence of 11βHSD1 was supported by elevated liver mRNA levels of *Col1a1* (Figure 4B). In keeping with enhanced myofibroblast activation, Western blot analysis showed that αSMA protein levels were higher at 24h and stayed elevated at 8d in GKO mice (Supporting Fig.S2B). Similarly, histological quantification of αSMA immunostaining showed that the GKO mice retained higher αSMA during the resolution phase (72h; Fig. 4A), although no histological difference was detected at peak fibrosis. In addition, *Acta2* (αSMA) gene

expression remained higher in GKO mice during resolution (72h; Fig. 4C). To identify whether the observed alteration in myofibroblast phenotype was specific to HSCs, we stained for reelin (Fig. 4D), a known marker of HSCs (29). We did not detect any significant difference in the number of reelin positive cells at 72h, the critical point in which markers of fibrosis were elevated in the GKO mice. Hence, no definitive conclusion could be drawn on the origins of myofibroblasts in this model.

GKO mice show similar hepatocellular damage after chronic or acute liver injury

To assess whether the exaggerated pro-fibrotic response in GKO mice following chronic CCl4 was due to more severe hepatocyte injury, we performed a detailed histopathological evaluation. This showed similar NAS inflammation, hepatocellular necrosis and total injury scores in GKO and control mice (Supporting Fig.S3A-C). In fact, plasma ALT and AST levels were lower in GKO mice compared to control injured mice during peak fibrosis (Fig. 4E-F). Plasma albumin levels were comparable between genotypes at peak injury 24h time point (control *vs* GKO: 25.40±2.12U/l *vs* 22.80±0.66U/l) and remained at similar levels throughout the resolution phases (data not shown).

To further evaluate the effects of global 11βHSD1-deficiency on hepatocellular injury, a single dose of CCl4 was administered to induce acute liver injury. As in the chronic CCl4 model, the GKO mice showed significantly lower plasma ALT, AST, ALP but similar albumin levels (Supporting Fig. S4A-D). The single dose confirmed similar histopathology scores between genotypes (Supporting Fig. S5A-C). Quantification of hepatocyte necrotic cell area using PAS staining showed similar degrees of hepatocellular death in GKO and control mice (Supporting Fig.S5D).

GKO mice show similar hepatic macrophage or neutrophil numbers to control mice in CCl4 injury

Apart from HSCs, macrophages have been implicated in both promoting fibrosis and facilitating resolution, therefore we further assessed if global 11βHSD1 deletion affects hepatic macrophages and neutrophil numbers during injury and resolution phases. Neutrophil

numbers were similar between GKO and control livers at all time points (Fig. 5A-B). Macrophage numbers (Fig. 5A-C) and cytokine mRNA levels of *Mcp1* and *Il1* (Fig. 5D-E) were also similar in GKO and control mice. Taken together these data suggest that enhanced pro-fibrotic response in GKO mice is not due to exacerbated inflammation or macrophage-induced fibrosis but is more likely to reflect a direct effect on hepatic stellate cell activation pathways.

Myofibroblast/Stellate cell 11βHSD1 knockdown enhances fibrosis markers in response to chronic CCl4.

To distinguish between possible contributions of 11βHSD1 deficiency in MFB and hepatocytes to the pro-fibrotic phenotype, we generated 2 independent mouse models targeting 11βHSD1 in either hepatocytes or MFB/HSC. Mice with hepatocyte-specific deficiency in 11βHSD1 (LKO) showed almost complete (94-100% knock down) loss of 11βHSD1 (Supporting Fig. S6A-B). At 24h after chronic CCl_4 the LKO mice showed identical hepatic pro-fibrotic responses histologically (Fig. 6A), similar liver function test changes (Fig. 6B-C) and identical macrophage or neutrophil numbers (Fig. 6D-E) to control littermates. Thus, deletion of 11βHSD1 in hepatocytes does not mimic the changes in liver fibrosis in GKO mice.

To assess the specific role of 11βHSD1 in the regulation of MFB/HSCs in the CCl4 model, we used mice with MFB/HSC-specific 11βHSD1 knockdown (MFKD). HSCs isolated from MFKD mice, demonstrate a 50-60% reduction in 11βHSD1 expression *in vitro* (Supporting Fig. S6C-D) compared to littermate controls. Following chronic CCl4 administration, MFKD mice showed increased COL1 and αSMA immuno-staining (Fig.7A) and significantly higher *Acta2* mRNA (Fig.7B) levels at 24h post CCl4 liver injury. No significant difference was detected in PSR staining (Fig.7A) or plasma ALT/AST levels (Fig.7C-D) between genotypes. Enhanced myofibroblast activation in MFKD mice was also confirmed in *ex-vivo* primary HSCs from MFKD mice that showed significantly higher *Acta2* and *Col1a1* levels at days 2, 5 and 8 in culture (Fig. 7E-F).

Pharmacological 11βHSD1 inhibition increases MFB activation and early fibrosis, but enhances scar resolution

To address the clinical relevance of our findings for 11βHSD1 inhibitor therapies, and specifically test the potential intervention times (prophylactic/injury/repair) we used the 11βHSD1 inhibitor UE2316 in the CCl_4 liver fibrosis model (Fig. 7A). During CCl_4 administration, UE2316-treated animals had slightly lower body weights (Supporting Fig. S7A), as shown before (21), but no difference in liver-to-body weight ratio (Supporting Fig. S7B). Overall, as observed in GKO mice, UE2316 treatment throughout the period of CCl_4 administration exacerbated hepatic fibrosis measured 24h following termination of CCl_4, as shown by PSR staining (Fig. 7B) and collagen 1 (Fig. 7B) immunohistochemistry. UE2316 treatment throughout CCl_4 injury also inhibited later scar resolution, as shown by elevated PSR and collagen 1 up to 8 days post-CCl_4. The UE2316 treated group had higher αSMA as early as 6 hours after the last CCl_4 injection, but this normalized during later resolution (Fig. 7D). Furthermore, as seen in GKO mice, plasma ALT and AST levels were significantly lower at both peak injury (24 h) and late resolution (day 8) in the UE2316 group compared to vehicle (Fig. 7E-F).

In order to investigate the therapeutic potential of 11βHSD1 inhibition and/or dissect the effects on injury/repair phases we administered UE2316 only during scar resolution, i.e. commencing UE2316 48h following the final CCl_4 injection (Fig.7A).There was no significant difference in total collagen or collagen 1 deposition in the UE-R group (Fig. 7B-C) compared to vehicle control, but administering UE2316 during the resolution phase accelerated the reduction in the number of αSMA positive cells (Fig.7D) and reduced plasma ALT levels (Fig.7E) at day 8.

Discussion

Collectively, these data from a comprehensive series of liver fibrosis studies using mice with either global or myofibroblast-restricted 11βHSD1-deficiency, a translational study using a small molecule 11βHSD1 inhibitor and our *in vitro* work using primary HSCs, demonstrate that attenuation of 11βHSD1 activity within the hepatic myofibroblast population enhances a profibrogenic myofibroblast phenotype and promotes liver fibrogenesis. The profibrotic response most likely occurs in HSCs, and not in hepatocytes (LKO had no phenotype), and is mediated by suppression of glucocorticoid action via 11βHSD1inhibition. It is also evident that in all the models of liver injury that we assessed, 11βHSD1 is suppressed during injury. Therefore, administration of systemic 11βHSD1 inhibitors, drugs which are currently under investigation in Phase 2 clinical trials, to patient groups at risk of NAFLD or NASH, may have unpredictable adverse effects on liver fibrosis progression and regression.

The profibrotic responses in the GKO and pharmacological inhibition are not due to greater hepatocellular injury since histopathology and necrosis scores did not show marked differences in liver damage. Interestingly, biochemical markers of hepatocyte death – ALT and AST were reduced in 11βHSD1 global deficiency/inhibition. The lower ALT/AST at peak fibrosis in our study is currently unexplained. However, given the role of 11βHSD1 in the modulation of anti-inflammatory glucocorticoids, we speculate that this could relate to differential effects of reduced GC exposure (systemically versus locally). Indeed, administration of exogenous GC to patients has been shown to increase ALT and AST levels (30). Animal studies have also shown that GCs increase ALT activity (31,32), therefore reduced GC availability with 11βHSD1pharmacological inhibition/global genetic deficiency could explain the reduced ALT/AST. In the cell type (LKO, MFKD)-specific models, the ALT/AST levels were similar to littermate controls. Hence, ALT/AST levels may not always reflect the degree of hepatocellular damage and histological confirmation of changes should be sought where possible. Note that the ALT and AST levels differed in the respective control strains likely because of background stain and age differences; this does not change the interpretation of our data.

Hepatocyte-specific deletion of 11βHSD1 did not show any apparent effect on liver fibrosis or hepatic injury in the CCl4 injury model, ruling out hepatocytes as a key locus for

11βHSD1 in this context. Similarly in a fatty liver model, LKO mice failed to show significant metabolic abnormalities or a distinct phenotype from control littermates (33). It is possible that in global deficiency, compensatory hypothalamic-pituitary-adrenal (HPA) axis activation (due to increased GC clearance) or paracrine modulators could affect pro-fibrotic responses. For example, global 11βHSD1 deficiency or inhibition, but not hepatocyte-specific deficiency (33,34), leads to moderate weight loss, which may modulate injury responses in the liver by altered leptin signalling (35). This suggests that 11βHSD1 deficiency either in other organs, or in other cells within the liver, is important to modifying the injury response.

Our data using the MFKD mouse model and *ex-vivo* HSC data (from MFKD, GKO, UE2316) suggest that 11βHSD1 could be a key regulator of MFB/HSC function. Reduction of 11βHSD1 in MFB/HSC populations is permissive towards a profibrotic profile with increased collagen-1 (a GC target gene) and α-smooth muscle actin levels. The lack of a significant difference in PSR staining in the MFKD model could be due to residual levels (50-60% knock down) of 11βHSD1 in MFB/HSC. The inhibitory effects of glucocorticoids on pro-fibrotic genes have also been observed in other disease models where fibroblasts play a key role. For example, in TGFβ-stimulated human lung fibroblasts, glucocorticoid treatment significantly reduced extracellular matrix related genes (36). Glucocorticoids also inhibit the pro-inflammatory cytokine-induced proliferation of adult rat cardiac fibroblasts (37). In support of our data, dexamethasone treatment of HSCs resulted in a significant reduction of Tgf-β-Smad mediated signalling (38), the upstream regulator of matrix deposition by activated HSCs. Although the effects of MFKD, 11βHSD1 genetic deficiency and pharmacological inhibition suggest direct activation of HSCs *in vitro* and the fact that HSCs are the major source of myofibroblasts in hepatotoxic liver injury (CCl_4) (39,40), it is possible that other hepatic myofibroblast subpopulations could have contributed to the effects observed in our *in vivo* studies.

Hepatic inflammation is also closely linked to liver fibrosis. Liver macrophages are critical regulators of both fibrogenesis and scar resolution (3, 41). Glucocorticoids are well known for their anti-inflammatory properties, and 11βHSD1 is expressed in macrophages and other

inflammatory cells (42). Effects of 11βHSD1 on inflammation are highly context-dependent. For example, GKO mice show reduced inflammation in atheroma lesions and decreased MCP1 expression and macrophage numbers in adipose tissue (16) after high fat feeding, but enhanced responses in serum arthritis and chemically induced peritonitis and pleurisy (42), increased serum TNF-alpha and IL-6 levels when challenged with LPS (43) and enhanced hepatic inflammation in a NAFLD-diet inducing model (44). We suspected that the pro-fibrotic profile seen in GKO and UE2316 treated mice could be attributed to exaggerated inflammatory response to CCl_4. However, we did not find any elevation of key inflammatory markers or in either hepatic macrophage or neutrophil numbers. Therefore, in our model it is unlikely that 11βHSD1 deficiency plays a regulatory role on inflammatory cell function.

We have not excluded other mechanisms potentially affecting fibrosis. In contrast with permissive effects on liver fibrosis in CCl_4 injury, GKO mice showed protection from adipose tissue scarring after high fat feeding. This anti-fibrotic role is associated with enhanced angiogenesis and reduced hypoxia in the adipose tissue of GKO mice (17), consistent with their enhanced angiogenesis in models of ischemic or injured tissue (15,18, 45). In chronic liver disease several studies show that angiogenesis is key in fibrosis progression, with exaggerated pathological angiogenesis leading to enhanced fibrosis (46-49) .Therefore increased angiogenesis with reduced 11βHSD1 in the liver could contribute to the enhanced fibrosis we observed.

Our work for the first time provides insights of translational importance in the use of 11βHSD1 inhibitors in liver injury. Administration of UE2316 prior to injury recapitulates the profibrotic phenotype seen in the GKO and MFKD genetic models. UE2316 restricted to the recovery phase, after chronic injury had been stopped, seemed to modestly reduce markers of myofibroblast activation. This dichotomous function of 11βHSD1 during injury and resolution, suggests context-dependent treatment effects. Similar paradigms for other pathways are now becoming more evident in the literature. For example, a recent study using VEGF-neutralizing antibodies showed 2 opposing effects: prevented development of fibrosis but also disrupted hepatic fibrosis resolution and tissue repair. During fibrosis resolution, VEGF inhibition impaired liver sinusoidal permeability, which was associated

with reduced monocyte infiltration of fibrotic liver and delayed tissue repair (50). GCs have known angiostatic mechanisms and we have previously shown that 11βHSD1 inhibition enhances VEGF expression which might be necessary during ECM remodelling at the scar resolution phase.

Selective 11βHSD1 inhibitors have been tested in phase II trials of obese patients with type 2 diabetes, but the modest size of their effects on glycemic control have stalled their commercial progress, and led to consideration of alternative/added indications, including NAFLD (13). From these preclinical data we cannot predict the consequences of 11βHSD1 inhibition for liver injury, and this requires more careful investigation. From a therapeutic point of view, it appears that administration of 11βHSD1 inhibitors prior to injury (as a prophylactic measure) might reduce transaminases levels but will perhaps be permissive towards fibrosis and delay collagen degradation. In contrast, if it were possible to administer 11βHSD1 inhibitors specifically during scar resolution, this may assist extracellular matrix remodelling.

Acknowledgements. We thank Drs Andrew McBride and Karen Sooy for advice on the preparation of UE2316 diets and the staff in the BRR facility (Edinburgh) for maintenance of the mouse colonies. We wish to thank Professor Jonathan Seckl for generous provision of GKO mice.

References

1. Tsuchida T & Friedman SL. Mechanisms of stellate cell activation. Nat Rev Gastroenterol Hepatol. 2017 ;14(7):397-411.

2. Iredale, J. P., R. C. Benyon, et al. Mechanisms of spontaneous resolution of rat liver fibrosis - Hepatic stellate cell apoptosis and reduced hepatic expression of metalloproteinase inhibitors. Journal of Clinical Investigation. 1998;102: 538-549

3. Ramachandran P, Pellicoro A, Vernon MA, Boulter L, Aucott RL, Ali A, et al. Differential Ly-6C expression identifies the recruited macrophage phenotype, which orchestrates the regression of murine liver fibrosis. Proc Natl Acad Sci U S A. 2012;109(46):E3186-195.

4. Wynn T.A. Cellular and molecular mechanisms of fibrosis. J Pathol. 2008; 214:199-210.

5. Hayden T. Scarred by disease. Nat Med. 2011;17:18-20.

6. Fede G, Spradaro L, Tomaselli T, Privitera G, Germani G, Tsochatzis E, et al. Adrenocortical dysfunction in liver disease. A systemic review. Hepatology. 2012;55(4):1282-91.

7. **Seckl JR, Walker BR**. Minireview: 11beta-hydroxysteroid dehydrogenase type 1- a tissue-specific amplifier of glucocorticoid action. Endocrinology. 2001;142(4):1371-1376.

8. Morton NM, Holmes MC, Fiévet C, Staels B, Tailleux A, Mullins JJ, Seckl JR. Improved lipid and lipoprotein profile, hepatic insulin sensitivity, and glucose tolerance in 11beta-hydroxysteroid dehydrogenase type 1 null mice. J Biol Chem. 2001; 276:41293-41300.

9. Paterson JM, Morton NM, Fievet C, Kenyon CJ, Holmes MC, Staels B, Seckl JR, Mullins JJ. Metabolic syndrome without obesity: Hepatic overexpression of 11beta-hydroxysteroid dehydrogenase type 1 in transgenic mice. Proc Natl Acad Sci U S A. 2004;101(18):7088-7093.

10. Konopelska S, Kienitz T, Hughes B, Pirlich M, Bauditz J, Lochs H, et al. Hepatic 11beta-HSD1 mRNA expression in fatty liver and nonalcoholic steatohepatitis. Clinical Endocrinology. 2009;70(4): 554-560.

11. Ahmed A, Rabbitt E, Brady T, Brown C, Guest P, Bujalska IJ, et al. A Switch in Hepatic Cortisol Metabolism across the Spectrum of Non Alcoholic Fatty Liver Disease. Plos One. 2012;7(2): e29531.

12. Anderson A, Walker BR. 11β-HSD1 inhibitors for the treatment of type 2 diabetes and cardiovascular disease. Drugs. 2013;73(13):1385-193.

13. Stefan N, Ramsauer M, Jordan P, Nowotny B, Kantartzis K, Machann J, Hwang JH et al. Inhibition of 11β-HSD1 with RO5093151 for non-alcoholic fatty liver disease: a multicentre, randomised, double-blind, placebo-controlled trial. Lancet Diabetes Endocrinol. 2014; 2:406-416.

14. Kotelevtsev Y, Holmes MC, Burchell A, Houston PM, Schmoll D, Jamieson P, et al. 11beta-hydroxysteroid dehydrogenase type 1 knockout mice show attenuated glucocorticoid-inducible responses and resist hyperglycemia on obesity or stress. Proc Natl Acad Sci U S A. 1997; 94(26): 14924-14929.

15. Small GR, Hadoke PW, Sharif I, Dover AR, Armour D, Kenyon CJ, et al. Preventing local regeneration of glucocorticoids by 11beta-hydroxysteroid dehydrogenase type 1 enhances angiogenesis. Proc Natl Acad Sci U S A. 2005; 102(34): 12165-12170.

16. **Wamil M, Battle JH**, Turban S, Kipari T, Seguret D, de Sousa Peixoto R, et al. Novel fat depot-specific mechanisms underlie resistance to visceral obesity and inflammation in 11 beta-hydroxysteroid dehydrogenase type 1-deficient mice Diabetes 2011; 60(4): 1158-1167.

17. Michailidou Z, Turban S, Miller E, Zou X, Schrader J, Ratcliffe PJ, et al. Increased Angiogenesis Protects against Adipose Hypoxia and Fibrosis in Metabolic Disease-resistant 11 beta-Hydroxysteroid Dehydrogenase Type 1 (HSD1)-deficient Mice. Journal of Biological Chemistry. 2012;287(6): 4188-4197.

18. Kipari T, Hadoke PW, Iqbal J, Man TY, Miller E, Coutinho AE, et al. 11β-hydroxysteroid dehydrogenase type 1 deficiency in bone marrow-derived cells reduces atherosclerosis. FASEB J. 2013;27(4):1519-1531

19. White CI, Jansen MA, McGregor K, Mylonas KJ, Richardson RV, Thomson A, et al. Cardiomyocyte and Vascular Smooth Muscle-Independent 11β-Hydroxysteroid Dehydrogenase 1 Amplifies Infarct Expansion, Hypertrophy, and the Development of Heart Failure After Myocardial Infarction in Male Mice. Endocrinology. 2016 157(1):346-357.

20. Henderson NC, Arnold TD, Katamura Y, Giacomini MM, Rodriguez JD, McCarty JH, et al. Targeting of αv integrin identifies a core molecular pathway that regulates fibrosis in several organs. Nat Med. 2013;19(12):1617-1624.

21. Sooy K, Noble J, McBride A, Binnie M, Yau JL, Seckl JR, et al. Cognitive and Disease-Modifying Effects of 11β-Hydroxysteroid Dehydrogenase Type 1 Inhibition in Male Tg2576 Mice, a Model of Alzheimer's Disease. Endocrinology. 2015;156:4592-4603.

22. Macfarlane DP, Zou X, Andrew R, Morton NM, Livingstone DE, Aucott RL, et al. Metabolic pathways promoting intrahepatic fatty acid accumulation in methionine and choline deficiency: implications for the pathogenesis of steatohepatitis. Am J Physiol Endocrinol Metab. 2011;300:E402-409.

23. Pellicoro A, Aucott RL, Ramachandran P, Robson AJ, Fallowfield JA, Snowdon VK, et al. Elastin accumulation is regulated at the level of degradation by macrophage metalloelastase (MMP-12) during experimental liver fibrosis.Hepatology 2012; 55(6): 1965-1975.

24. Kleiner DE, Brunt EM, Van Natta M, Behling C, Contos MJ, Cummings OW, et al. Design and validation of a histological scoring system for nonalcoholic fatty liver disease. Hepatology. 2005; 41(6):1313-21.

25. Turban S, Liu X, Ramage L, Webster SP, Walker BR, Dunbar DR, et al. Optimal elevation of beta-cell 11beta-hydroxysteroid dehydrogenase type 1 is a compensatory mechanism that prevents high-fat diet-induced beta-cell failure.Diabetes. 2012;61(3): 642-652.

26. Rajan V, Chapman KE, Lyons V, Jamieson P, Mullins JJ, Edwards CR, Seckl JR. Cloning, sequencing and tissue-distribution of mouse 11 beta-hydroxysteroid dehydrogenase-1 cDNA. J Steroid Biochem Mol Biol. 1995;52:141-147.

27. Nixon M, Wake DJ, Livingstone DE, Stimson RH, Esteves CL, Seckl JR, Chapman KE, Andrew R, Walker BR. Salicylate downregulates 11β-HSD1 expression in adipose tissue in obese mice and in humans, mediating insulin sensitization. Diabetes. 2012;61:790-796.

28. L Xu, A Y Hui, E Albanis, M J Arthur, S M O'Byrne, W S Blaner, P Mukherjee, S L Friedman, F J Eng. Human hepatic stellate cell lines, LX-1 and LX-2: new tools for analysis of hepatic fibrosis. Gut. 2005; 54: 142–151.

29. Kobold D, Grundmann A, Piscaglia F, Eisenbach C, Neubauer K, Steffgen J, Ramadori G, Knittel T. Expression of reelin in hepatic stellate cells and during hepatic tissue repair: a novel marker for the differentiation of HSC from other liver myofibroblasts. J Hepatol. 2002 ;36(5):607-613.

30. Moleti M, Giuffrida G, Sturniolo G, Squadrito G, Campennì A, Morelli S, et al. Acute liver damage following intravenous glucocorticoid treatment for Graves' ophthalmopathy. Endocrine. 2016;54(1):259-268

31. Reagan WJ, Yang RZ, Park S, Goldstein R, Brees D Gong D. Metabolic Adaptive ALT Isoenzyme Response in Livers of C57/BL6 Mice Treated with Dexamethasone. Toxicol Pathol. 2012; 40(8): 1117–1127.

32. Qian K, Zhong S, Xie K, Yu D, Yang R, Gong D. Hepatic ALT isoenzymes are elevated in gluconeogenic conditions including diabetes and suppressed by insulin at the protein level. Diabetes Metab Res Rev. 2015; 31(6): 562–571.

33. Lavery GG, Zielinska AE, Gathercole LL, Hughes B, Semjonous N, Guest P, et al. Lack of significant metabolic abnormalities in mice with liver-specific disruption of 11β-hydroxysteroid dehydrogenase type 1. Endocrinology. 2012;153:3236-3248.

34. Morgan SA, McCabe EL, Gathercole LL, Hassan-Smith ZK, Larner DP, Bujalska IJ, et al. 11β-HSD1 is the major regulator of the tissue-specific effects of circulating glucocorticoid excess. Proc Natl Acad Sci U S A. 2014;111(24):E2482-91

35. Polyzos SA, Kountouras J, Mantzoros CS. Leptin in nonalcoholic fatty liver disease: a narrative review. Metabolism. 2015;64(1):60-78.

36. Todorova L, Gürcan E, Westergren-Thorsson G, Miller-Larsson A. Budesonide/formoterol effects on metalloproteolytic balance in TGFbeta-activated human lung fibroblasts. Respir Med 2009;103(11): 1755-1763.

37. He YH, Zhang HN, Zhang GP, Hou N, Xiao Q, Huang Y, et al. A physiological concentration of glucocorticoid inhibits the pro-inflammatory cytokine-induced proliferation of adult rat cardiac fibroblasts: roles of extracellular signal-regulated kinase 1/2 and nuclear factor-kappaB. Clin Exp Pharmacol Physiol. 2011;38(11): 739-746.

38. Bolkenius U, Hahn D, Gressner AM, Breitkopf K, Dooley S, Wickert L. Glucocorticoids decrease the bioavailability of TGF-beta which leads to a reduced TGF-beta signaling in hepatic stellate cells. Biochemical and Biophysical Research Communications. 2004;325(4): 1264-1270.

39. Mederacke I, Hsu CC, Troeger JS, Huebener P, Mu X, Dapito DH, et al. Fate tracing reveals hepatic stellate cells as dominant contributors to liver fibrosis independent of its aetiology. Nat Commun 2013;4:2823-2835.

40. Iwaisako K, Jiang C, Zhang M, Cong M, Moore-Morris TJ, Park TJ, et al. Origin of myofibroblasts in the fibrotic liver in mice. Proc Natl Acad Sci U S A. 2014;111(32):E3297-305.

41. Bataller, R. and D. A. Brenner. Liver fibrosis. Journal of Clinical Investigation. 2005;115(2): 209-218.

42. Coutinho AE, Gray M, Brownstein DG, Salter DM, Sawatzky DA, Clay S, et al. 11β-Hydroxysteroid dehydrogenase type 1, but not type 2, deficiency worsens acute inflammation and experimental arthritis in mice. Endocrinology. 2012;153(1):234-40.

43. Zhang, T. Y. and R. A. Daynes. Macrophages from 11 beta-hydroxysteroid dehydrogenase type 1-deficient mice exhibit an increased sensitivity to lipopolysaccharide stimulation due to TGF-beta-Mediated up-regulation of SHIP1 expression. Journal of Immunology. 2007;179: 6325-6335.

44. Larner DP, Morgan SA, Gathercole LL, Doig CL, Guest P, Weston C, et al. Male 11β-HSD1 Knockout Mice Fed Trans-Fats and Fructose Are Not Protected From Metabolic Syndrome or Nonalcoholic Fatty Liver Disease . Endocrinology. 2016;157:3493-504.

45. McSweeney SJ, Hadoke PW, Kozak AM, Small GR, Khaled H, Walker BR, Gray GA, et al. Improved heart function follows enhanced inflammatory cell recruitment and angiogenesis in 11 beta HSD1-deficient mice post-MI. Cardiovascular Research. 2010; 88(1): 159-167.

46. Medina J, Arroyo AG, Sanchez-Madrid F, Moreno-Otero R. Angiogenesis in chronic inflammatory liver disease. Hepatology. 2004; 39: 1185–1195.

47. Tugues S, Fernandez-Varo G, Munoz-Luque J, Ros J, Arroyo V, et al. Antiangiogenic treatment with sunitinib ameliorates inflammatory infiltrate, fibrosis, and portal pressure in cirrhotic rats. Hepatology.2007;46: 1919–1926.

48. Lee JS, Semela D, Iredale J, Shah VH. Sinusoidal remodeling and angiogenesis: a new function for the liver-specific pericyte? Hepatology. 2007;45: 817–825.

49. Taura K, De Minicis S, Seki E, Hatano E, Iwaisako K, Osterreicher CH, et al. Hepatic stellate cells secrete angiopoietin 1 that induces angiogenesis in liver fibrosis. Gastroenterology. 2008;135(5): 1729-1738

50. Yang L, Kwon J, Popov Y, Gajdos GB, Ordog T, Brekken RA, et al. Vascular endothelial growth factor promotes fibrosis resolution and repair in mice. Gastroenterology. 2014;146(5):1339-1350.

HEP-16-2216R2 Zou et al, **11βHSD1 deficiency or inhibition enhances hepatic myofibroblast activation in murine liver fibrosis**

Figure legends

Fig.1: Reduced 11βHSD1 expression in mouse models of liver fibrosis. Hepatic 11βHSD1mRNA levels measured by real time PCR (A) and protein levels (B), with upper panel showing representative immunoblot for 11βHSD1and GAPDH and lower panel quantification graph, during peak (48h) and resolution (1week, 1month) phases in the reversible CCl_4 (A,B) and TAA (C) liver fibrosis models, n=6/group. (D) Hepatic *Hsd11b1* mRNA levels in control (Con) diet, choline-deficient (CDD) and methionine-deficient (MCDD) NASH models, assessed by in situ mRNA hybridization (quantification graph showing average grain counts per area) n=6/group* $p<0.05$; ** $p<0.01$; *** $p<0.001$ compared to the vehicle group (A-C). $^{+}p<0.05$, $^{+++}p<0.001$ compared to the 48 hour injury time point.

Fig.2: Reduced 11βHSD1 expression during HSC activation *in vitro.* Expression levels of 11βHSD1 and α-SMA during *ex-vivo* wild type mouse HSC activation *in vitro* (n=3/group). (A) α-SMA protein, (B) *Hsd11b1* mRNA, (C) 11βHSD1 protein and (D) 11βHSD1 enzymatic activity (% conversion 11-dehydrocorticosterone to corticosterone) were measured during 2-11 days post activation. Comparison of *Acta2* (E) and *Col1a1* (F) mRNA levels in wild type (white bars) and GKO (black bars) HSCs during 2-11days post activation. * $p<0.05$; ** $p<0.01$; *** $p<0.001$ * compared to basal day 2 (A-D) or between genotypes within a time point (E-F); $^{+++}p<0.001$ comparisons between day 5 and 8 (D).

Fig.3: Glucocorticoid inhibition of profibrotic gene expression is amplified by 11βHSD1 in murine HSCs *in vitro*. mRNA levels of *Acta2* (A) and *Col1α1* (B) in C57Bl6/J HSCs in primary culture for 8 days and treated with combinations of vehicle (white bars), 500nM 11-dehydrocorticosterone (compound 'A', vertical stripped bars), 500nM corticosterone (compound 'B', horizontal stripped bars), 10μM UE2316 (compound 'U'; grey bars_), and

combination of A+B (black bars). Levels of mRNAs of interest are expressed relative to 18S RNA. Experiments were conducted in triplicate: * $p<0.05$; ** $p<0.01$.

Fig.4: Increased fibrotic response in livers of global 11βHSD1-deficient (GKO) mice after CCl_4 administration. GKO (black bars) and wild type (white bars) mice were administered twice weekly ip injections of CCl_4 for 12 weeks. 24h time point represents the peak injury and 72h-8d is the scar resolution phase. (A) Representative images of total collagen (picrosirius red, PSR), and smooth muscle actin (αSMA) staining during injury (24h) and resolution (72h and 8 days) phases, with arrowheads pointing to intense collagen staining and smooth muscle actin positive cells in control and GKO mice. Quantification of staining for PSR and αSMA are shown below the corresponding panel of representative images. Pixels of 30-40 continuous fields (x80) from each section were randomly selected and measured. Hepatic levels of *Col1a1* (B), and *Acta2* mRNA (C) were measured by qPCR and normalized for 18S. (D) Representative images (scale bar 100μm) and quantification graph of reelin immunohistochemistry (at 72h) to identify hepatic stellate cells. Plasma levels of alanine (ALT; E) and aspartate (AST; F) aminotransferases during injury and resolution phases. N=5-6 in each group; * $p<0.05$; ** $p<0.01$; *** $p<0.001$ between genotypes within time points.

Fig. 5: **Similar inflammatory responses to control mice in GKO following CCl_4 liver injury.** (A) A panel of representative flow cytometry images gating for $Ly6G^+$ $CD11b^+$ cells (neutrophils) and $F4/80^+$ $CD11b^+$ cells (macrophages) with quantification graphs (at the bottom of each representative image panel) for inflammatory cells as % of neutrophils and macrophages among all non-parenchymal cells in the liver. Hepatic levels of mRNAs encoding MCP-1 (B) and IL-1beta (C) quantified by qPCR and normalized for 18S in control (white bars) and GKO mice (black bars). There were no differences between groups (n=6/group).

HEP-16-2216R2 Zou et al, **11βHSD1 deficiency or inhibition enhances hepatic myofibroblast activation in murine liver fibrosis**

Fig.6: Mice with hepatocyte-specific 11βHSD1-deficiency (LKO) and their littermate controls show similar hepatic responses to CCl_4 injury. (A) Representative images of total collagen (picrosirius red, PSR), collagen 1 (Col1) and α-smooth muscle actin (αSMA) staining at 24h peak injury in control and LKO mice with quantification graphs at the bottom of each representative image panel. Plasma levels of ALT (B) and AST (C) in control (*Hsd11b1*$^{fl/fl}$; white bars) and LKO (black bars) mice during injury. There were no differences between groups (n=6/group). Control (white bars) and LKO (black bars) liver sections were stained for neutrophils GR-1 (Ly6G) (D) and macrophages (F4/80) (E). 20-30 consecutive fields with magnification *400 were quantified for each section. Cell number of each field was counted by an investigator, who was blinded for the genotype and treatment of the section. The average of cell number per field was calculated. There were no differences between groups (n=5-6/group).

Fig.7: **Knock-down of 11βHSD1 specifically in HSC/MF populations (MFKD) enhances hepatic myofibroblast activation and fibrotic response in CCl4 injury.** Male mice (10-12 weeks old) were administered CCl4 i.p. for 12 weeks to induce liver injury (n=6/group)**.** (A) Representative images of total collagen (picrosirius red, PSR), collagen 1 (Col1) and α-smooth muscle actin (αSMA) staining at 24h peak injury in control and MFKD mice with quantification graphs at the bottom of each representative image panel.(B) Hepatic *Acta2* mRNA levels were measured by qPCR and normalized for 18S. Plasma levels of ALT (C) and AST (D) in control (*Hsd11b1*$^{fl/fl}$; white bars) and MFKD (black bars) mice during injury. HSCs were isolated from 8 week old mice. *Acta2* (E) and *Col1a1* (F) mRNA levels were measured during 2-5-8 days post *ex-vivo* HSC activation in MFKD (black bars) and control littermates (white bars) (n=3/group). * $p<0.05$; ** $p<0.01$; *** $p<0.001$ comparisons between genotypes.

HEP-16-2216R2 Zou et al, **11βHSD1 deficiency or inhibition enhances hepatic myofibroblast activation in murine liver fibrosis**

Fig.8: Inhibition of 11βHSD1 in mice enhances the early liver fibrotic response to CCl_4 but when restricted to the repair phase, improves resolution of scarring. (A) Schematic view of the experimental design. Mice were administered twice weekly ip injections of CCl_4 for 12 weeks, and divided into 3 groups: a Chow diet (CD; white) group that was kept on vehicle diet for the duration of the experiment; a UE group (grey) that was kept on a diet containing the 11βHSD1 inhibitor UE2316 for the whole duration of the experiment; and a UE-R group (black) that started on a vehicle chow diet and switched to the UE diet 48h after the last CCL_4 injection. In this experiment a very early 6h time point was included to capture the earliest injury response. Representative images and quantification graphs of PSR (B), Col1 (C) and αSMA (D) staining were quantified in 30-40 continuous fields (x80) from each section of each group. Plasma levels of ALT (E) and AST (F) in mice treated with vehicle (white bars), UE (grey bars) or UE-R (black bars). N=5-6 in each group; * $p<0.05$; ** $p<0.01$; *** $p<0.001$ tested by two-way ANOVA.

Supporting Fig.S1: 11βHSD1 levels in CCl_4 liver injury and in human HSCs in culture.

(A) 11βHSD1 activity in liver homogenates from the CCl_4 injury model (n=6/group) after vehicle or after 48 hours or 1 week of CCl_4 administration. (B) *Hsd11b1* mRNA levels were measured in human LX-2 HSC incubated in serum-free medium (n=3 replicates per treatment) and treated with vehicle or activated with TGF-β (2ng/ml) for 16h. * $p<0.05$ tested by one-way ANOVA (A) or T-test (B).

Supporting Fig.S2: Higher hepatic collagen 1 and αSMA protein levels in GKO in the CCl_4 injury model. . (A) Representative images and quantification graph of collagen 1 staining during injury (24h) and resolution (72h and 8 days) phases, with arrowheads pointing to intense collagen 1 staining in control (white bars) and GKO (black bars) mice. (B) Representative hepatic α-SMA western blot image and quantification graph in control and GKO mice at peak (24h) and resolution (72h, 8d) time points in the CCl_4 liver fibrosis model, n=6/group. * $p<0.05$; ** $p<0.01$ between groups tested by two-way ANOVA.

Supporting Fig.S3: Similar histopathology scores in GKO and control mice in chronic CCl4 injury model. GKO (black circles) and control (open circles) liver H&E stained sections from the 24h peak fibrosis time point were scored for (A) NAS inflammation (insert table showing the scoring system) (B) hepatocellular necrosis (insert table showing the scoring system) and (C) total liver injury was calculated by adding the scores from A and B. n=6/group. There was no ballooning or steatosis or Mallory bodies observed.

Supporting Fig.S4: GKO mice show lower plasma transaminases after acute single dose CCl4 injury compared to control mice. Plasma levels of alanine (ALT; A), aspartate (AST; B) aminotransferases and alkaline phosphatase (ALP; C) and albumin (D). n=6/group; * $p<0.05$; ** $p<0.01$ between genotypes tested with Student's t test.

Supporting Fig.S5: GKO mice have similar hepatocellular damage and necrotic areas after single dose CCL4 injury compared to control mice. GKO (black circles) and control (open circles) liver H&E stained sections from a single CCl4 dose were scored for (A) NAS inflammation (B) hepatocellular necrosis and (C) total liver injury was calculated by adding the scores from A and B. n=6/group. There was no ballooning or steatosis or Mallory bodies observed. (D)Representative images (scale bar 200μm) and quantification graph of Periodic acid-Schiff (PAS) stain in livers of control (white bars) and GKO mice (black bars). Pale blue stain indicates necrotic areas.

Supporting Fig.S6: Recombination efficiency in LKO and MFKD mouse models.(A) Hepatic *Hsd11b1* mRNA normalized for 18S and (B) 11β-HSD1 protein normalized for GAPDH in LKO mice shows almost complete 11β-HSD1 ablation compared to control (*Cre-*) littermates (n=6/group). *** $p<0.001$ between groups tested with Student's t-test. (C) *Hsd11b1* mRNA normalized for 18S in isolated HSCs from MFKD (black bars)and control littermates (white bars) during 2-5-8 days post *ex-vivo* HSC activation (n=3/group). For clarity only significant differences ** $p<0.01$; *** $p<0.001$ * between genotypes within a time point are shown. Note that as seen if Fig. 2B *Hsd11b1* mRNA is reduced during HSC

activation in control mice. (D) 11βHSD1 enzymatic activity (% conversion 11-dehydrocorticosterone to corticosterone) was measured at day 8 post HSC activation (n=5/group).

Supporting Fig.S7: Body and liver weights after UE2316 inhibitor administration. (A) body weight (BW) comparisons between chow diet (open circle) and UE2316 (black square) groups during the 12 week CCl4 injury model (B) liver weights corrected for BW between chow diet (white bars) and UE2316 (grey bars) and UE-R (black bars) groups during the 12 week CCl4 injury model. Repeated measures ANOVA, ** $p<0.01$; *** $p<0.001$ significant differences between groups.

FIGURE 1

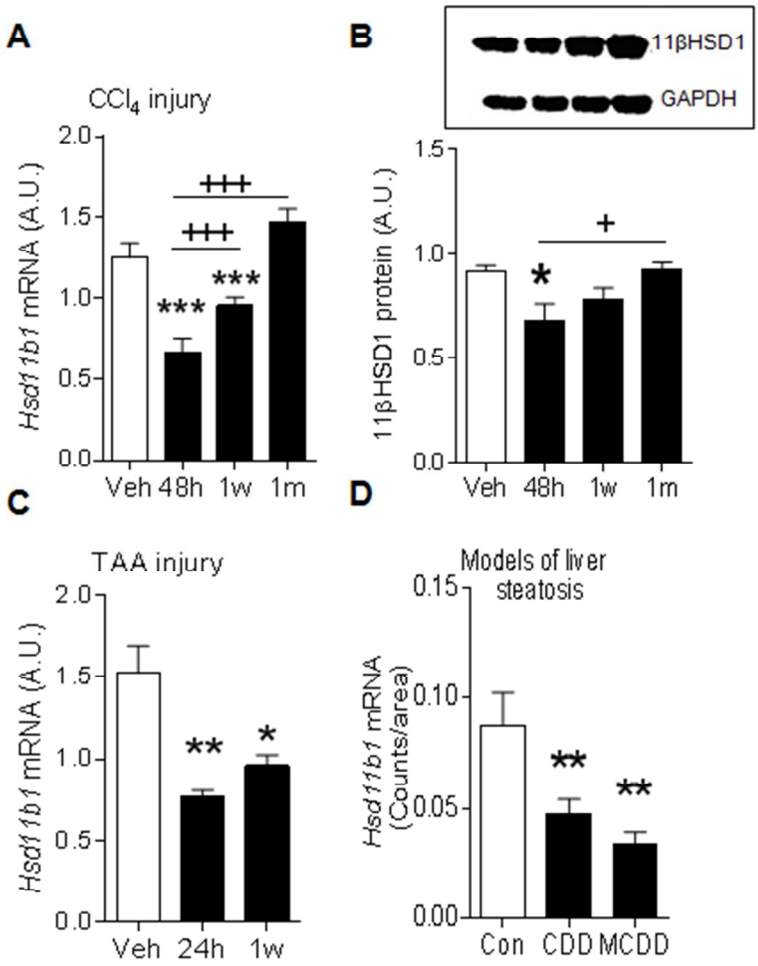

Reduced 11βHSD1 expression in mouse models of liver fibrosis

47x50mm (300 x 300 DPI)

FIGURE 2

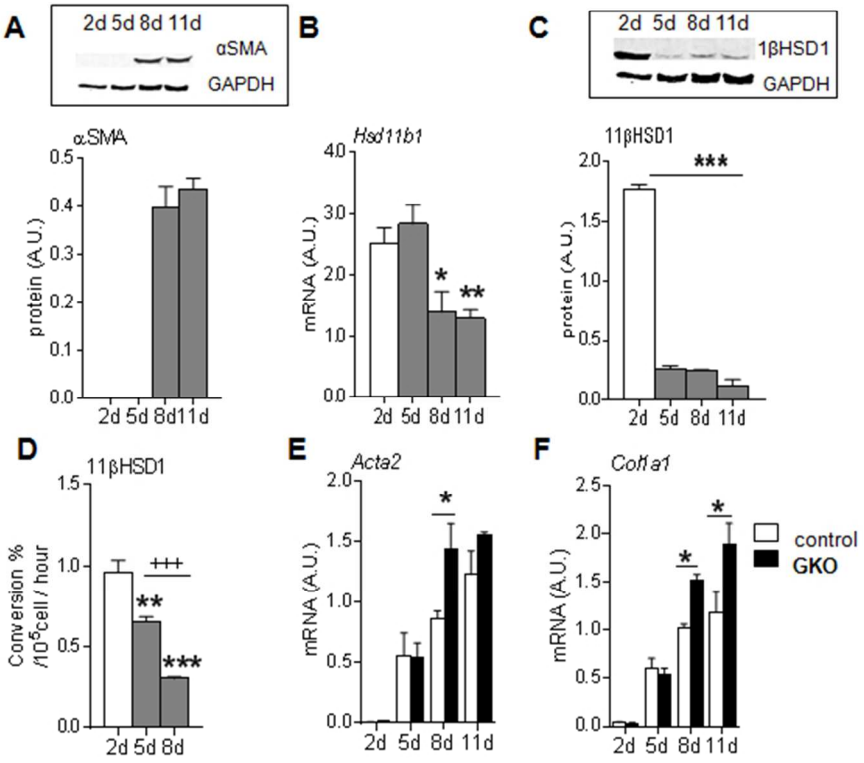

Reduced 11βHSD1 expression during HSC activation in vitro.

54x47mm (300 x 300 DPI)

FIGURE 3

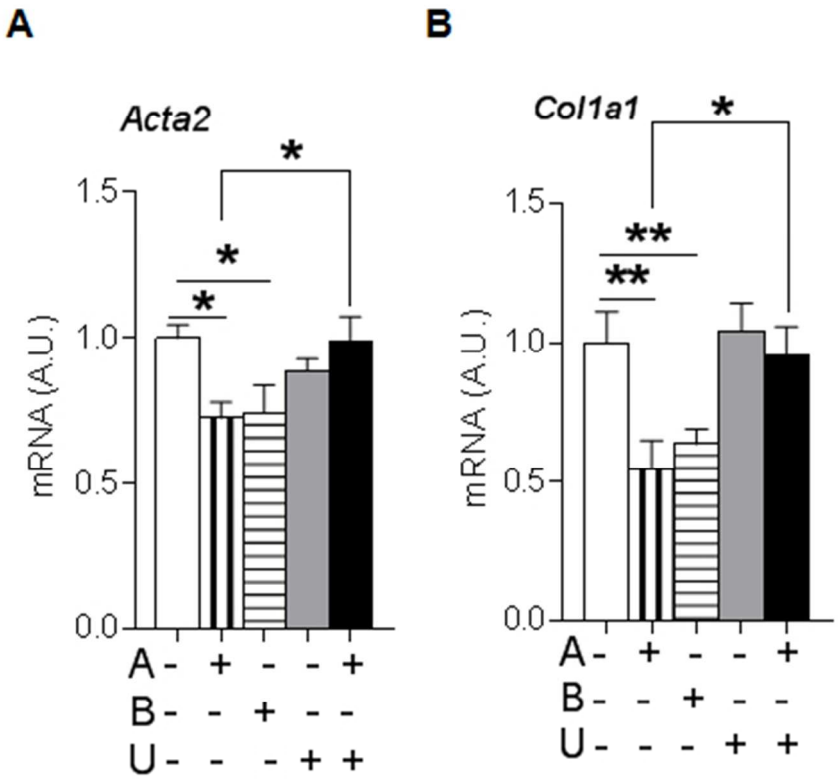

Glucocorticoid inhibition of profibrotic gene expression is amplified by 11βHSD1 in murine HSCs in vitro

36x39mm (300 x 300 DPI)

FIGURE 4

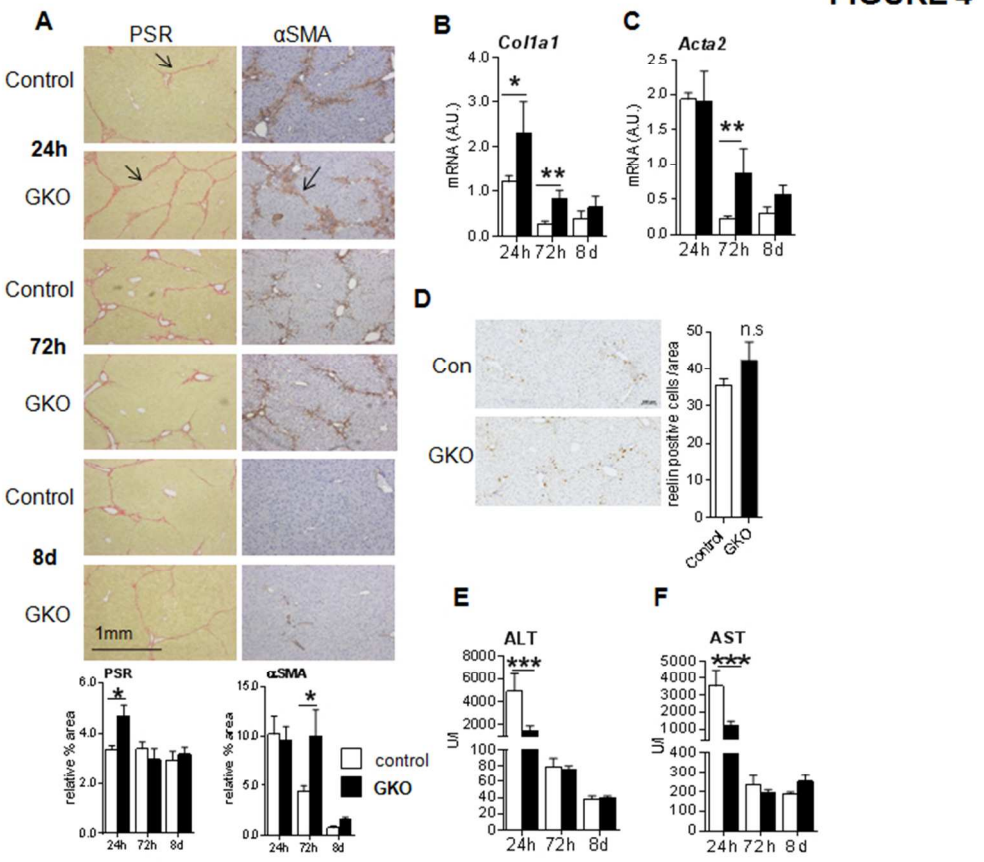

Increased fibrotic response in livers of global 11βHSD1-deficient (GKO) mice after CCl4 administration

64x58mm (300 x 300 DPI)

FIGURE 5

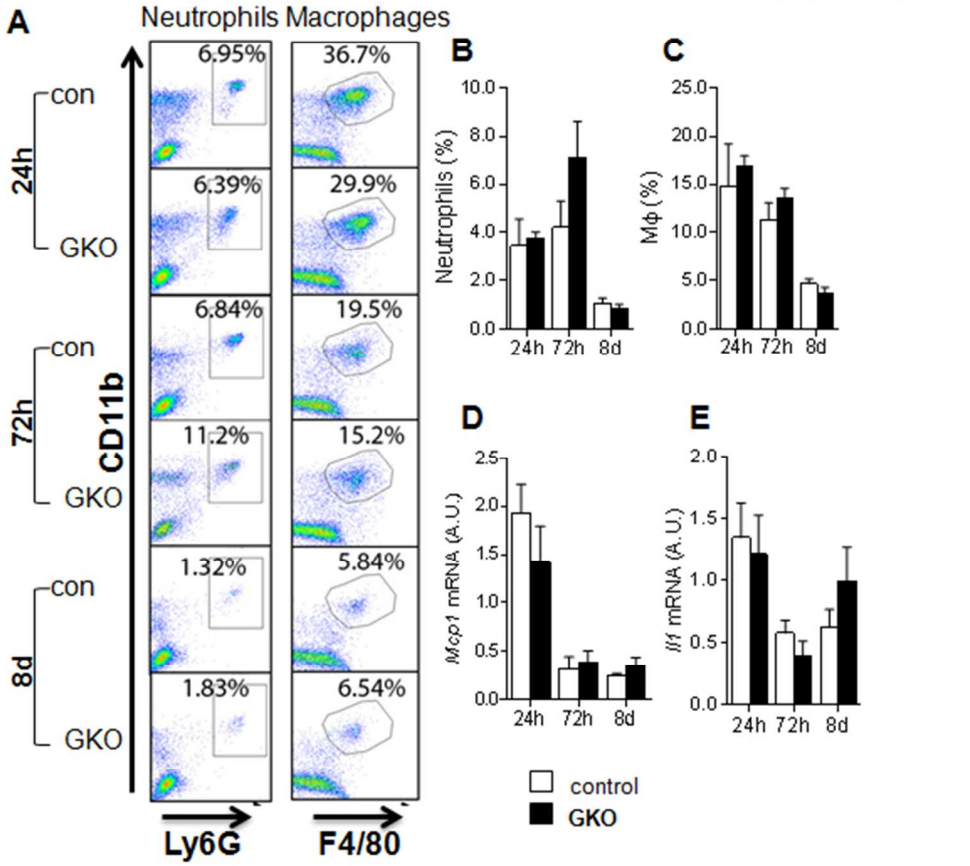

GKO mice have similar macrophage and neutrophil numbers to control mice after CCl4 injury

50x47mm (300 x 300 DPI)

FIGURE 6

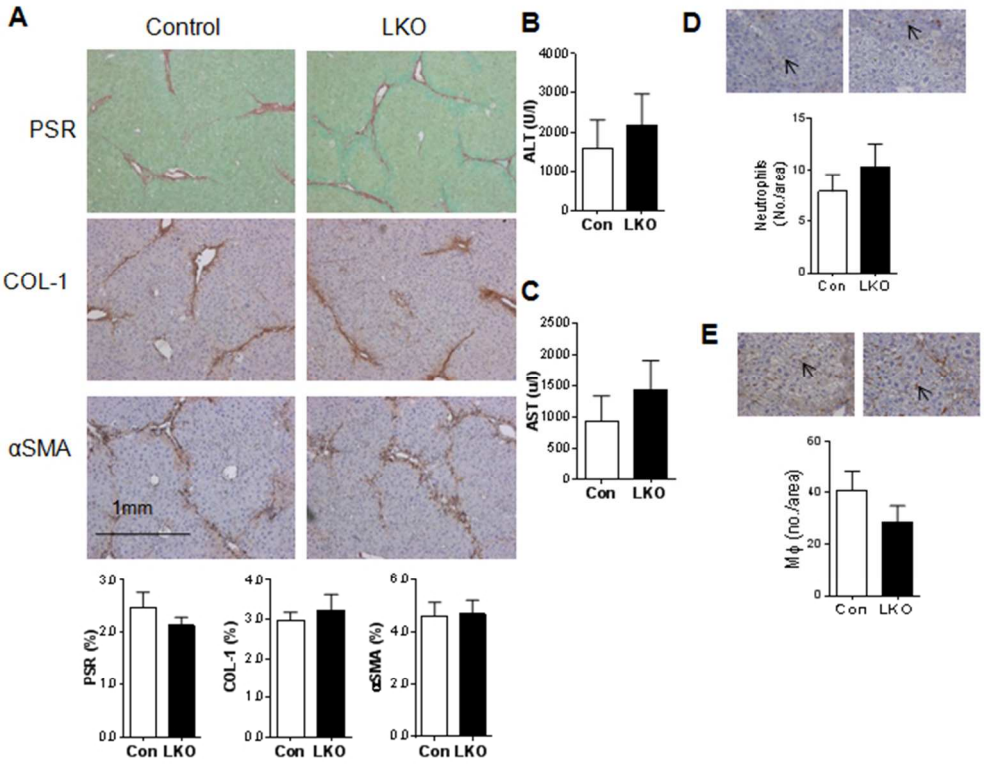

LKO mice show no apparent phenotype in CCl4 injury

59x53mm (300 x 300 DPI)

FIGURE 7

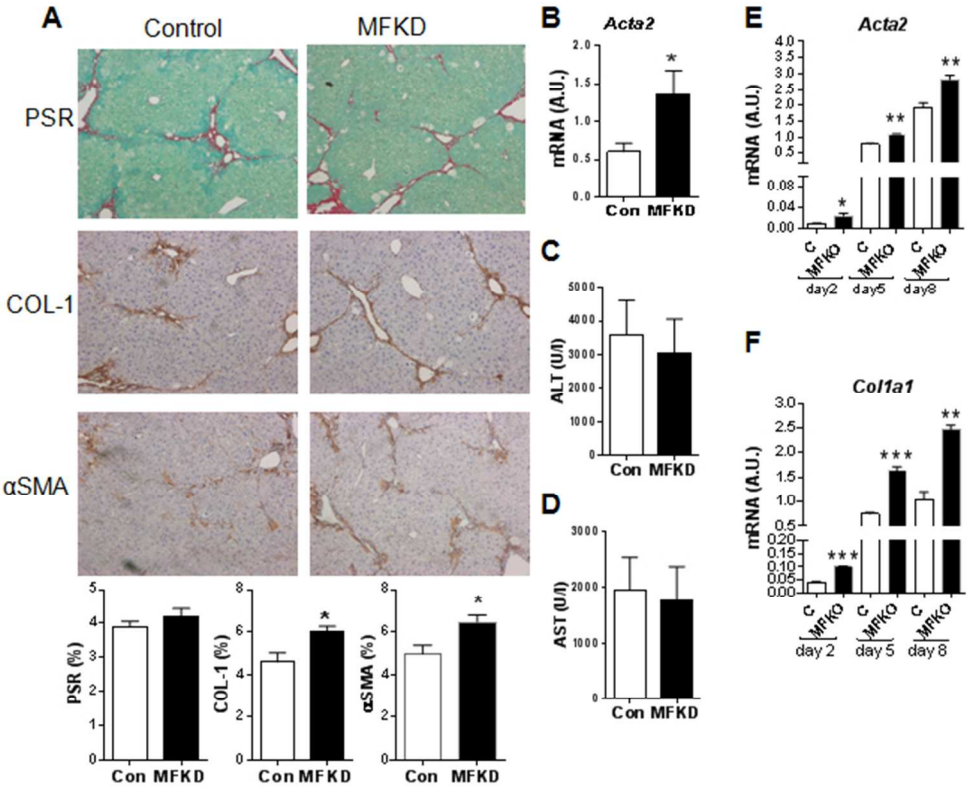

Myofibroblast/Stellate cell 11βHSD1 knockdown enhances fibrosis markers in CCl4 injury

56x51mm (300 x 300 DPI)

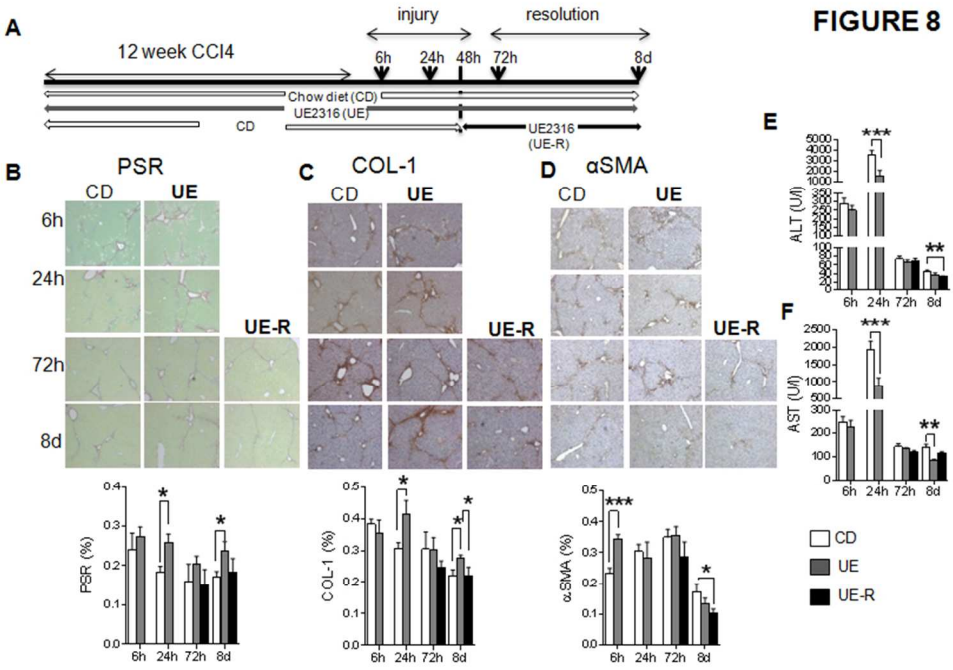

Inhibition of 11βHSD1 in mice enhances the early liver fibrotic response to CCl4 but when restricted to the repair phase, improves resolution of scarring

71x49mm (300 x 300 DPI)